Available online at www.sciencedirect.com
SCIENCE DIRECT®
Solar Energy 80 (2006) 895–907
SOLAR ENERGY
www.elsevier.com/locate/solener

Heat transfer and friction characteristics of rectangular solar air heater duct using rib-grooved artificial roughness

A.R. Jaurker [a,*], J.S. Saini [b], B.K. Gandhi [b]

[a] Mechanical Engineering Department, Government Engineering College, Jabalpur 482 011, MP, India
[b] Mechanical and Industrial Engineering Department, Indian Institute of Technology Roorkee, Roorkee 247 667, India

Received 4 March 2005; received in revised form 24 August 2005; accepted 29 August 2005
Available online 30 September 2005

Communicated by: Associate Editor Brian Norton

Abstract

Experimental investigation on the heat transfer and friction characteristics of rib-grooved artificial roughness on one broad heated wall of a large aspect ratio duct shows that Nusselt number can be further enhanced beyond that of ribbed duct while keeping the friction factor enhancement low. The experimental investigation encompassed the Reynolds number range from 3000 to 21,000; relative roughness height 0.0181–0.0363; relative roughness pitch 4.5–10.0, and groove position to pitch ratio 0.3–0.7. The effect of important parameters on the heat transfer coefficient and friction factor has been discussed and the results are compared with the results of ribbed and smooth duct under similar flow conditions. The present investigation clearly demonstrates that the heat transfer coefficient for rib-grooved arrangement is higher than that for the transverse ribs, whereas the friction factor is slightly higher for rib-grooved arrangement as compared to that of rectangular transverse ribs of similar rib height and rib spacing. The conditions for best performance have been determined. Correlations for Nusselt number and friction factor have been developed that predict the values within reasonable limits.

Keywords: Artificial roughness; Thermo-hydraulic performance; Heat transfer coefficient; Friction factor; Solar air heater; Aspect ratio

1. Introduction

It has been observed that the heat transfer coefficient between the absorber plate and working fluid of solar air heater is generally low. It is attributed to the formation of a very thin boundary layer at the absorber plate surface commonly known as viscous sub-layer. This convective heat transfer coefficient can be increased by providing the artificial roughness on the heat transferring surface (Webb, 1987). It has been found that the artificial roughness applied on the heat transferring surface breaks the viscous sub-layer, which reduces thermal resistance and promotes turbulence in a region close to artificially roughened surface. Although the application of artificial roughness in the duct of a conventional solar air heater has been shown to be an efficient method of enhancement of thermal efficiency of solar air heater, however, the use of artificial

* Corresponding author. Fax: +91 1332 285665.
E-mail address: ananddme@iitr.ernet.in (A.R. Jaurker).

0038-092X/$ - see front matter © 2005 Elsevier Ltd. All rights reserved.
doi:10.1016/j.solener.2005.08.006

Nomenclature

A_o	cross-section area of orifice, m^2
A_p	area of absorber plate, m^2
A_0	coefficient used in Eq. (8)
B_0	coefficient used in Eq. (9)
C_0, C_1, C_2	coefficients used in Eq. (10)
C_d	coefficient of discharge for orifice meter
C_p	specific heat of air at constant pressure, J/kg K
D	equivalent diameter of duct, m; $[D = 4WH/2(W + H)]$
D_0, D_1, D_2, D_3	coefficients used in Eq. (13)
e	rib height (or depth of groove), m
e/D	relative roughness height
g	groove position between ribs, m
g/p	groove position to pitch ratio
f_s	friction factor in smooth duct
f	friction factor in roughened duct
H	depth of duct, m
h	convective heat transfer coefficient, W/m^2 K
$(\Delta h)_o$	difference in levels of U-tube manometer, m
$(\Delta h)_d$	height of liquid in micro-manometer, m
k	thermal conductivity of air, W/m K
L_f	length of test section for pressure drop measurement, m
m	mass flow rate of air in duct, kg/s
Nu	Nusselt number for roughened duct
Nu_s	Nusselt number for smooth duct
p	pitch of rib (or groove), m
Pr	Prandtl number
p/e	relative roughness pitch
$(\Delta P)_d$	pressure drop across duct test section, N/m^2
$(\Delta P)_o$	pressure drop across orifice meter, N/m^2
Q_u	useful heat gain, W
Re	Reynolds number ($Re = VD/\upsilon$)
T_f	mean temperature of air, K
T_i	inlet temperature of air, K
T_o	outlet air temperature, K
T_p	average plate temperature, K
V	velocity of air in duct, m/s
υ	kinematic viscosity of air, m^2/s^2
W	width of duct, m
w	width of rib, m
β	ratio of orifice diameter to pipe diameter
θ	tilt angle of manometer, degree
ρ	density of air, kg/m^3
ρ_m	density of manometer fluid (methyl alcohol), kg/m^3

roughness results in higher friction losses leading to excessive power requirement for the air flow through the duct. It is therefore desirable that the turbulence must be created only in the region very close to the heat transferring surface i.e. in the viscous sub-layer only where the heat transfer takes place and the core flow should not be unduly disturbed so as to avoid excessive friction losses. This can be done by keeping the height of the roughness elements to be small in comparison with the duct dimensions (Saini, 2004). The use of artificial roughness in solar air heaters owes its origin to several investigations carried-out in connection with the enhancement of heat transfer in nuclear reactors, cooling of turbine blades and electronic components. Nikuradse (1950) and Dipprey and Sabersky (1963) developed friction similarity law for heat and momentum transfer analogy for fluid flow in rough pipes. Webb et al. (1971) developed heat transfer and friction factor correlations for turbulent air flow in tubes having rectangular repeated rib roughness. Han and Park (1988) and Han et al. (1989) conducted extensive experiments to simulate the flow through turbine blades. For developing and fully developed turbulent flow, heat transfer and friction characteristics of ducts with rib turbulators on two opposite walls of the square and rectangular ducts have been extensively studied. The results show that angled or inclined ribs give higher heat transfer than transverse ribs, and narrow aspect ratio ducts perform better than wide aspect ratio ducts. The angled ribs give higher heat transfer rate than the transverse ribs because of the secondary flow induced by the rib, in addition to breaking the viscous sub-layer and producing local wall turbulence. The concept of combined turbulence promoters in the form of rib-groove, with groove at the centre of ribs was introduced by Zhang et al. (1994). Their results show that the heat transfer performance of the rib-grooved roughened duct is much better than that of the rib-roughened duct. The rib-grooved roughened walls enhance the heat transfer 3.4 times and pay six times the pressure drop pen-

alty, whereas the rib roughened walls, with similar rib height and rib spacing, enhance the heat transfer 2.4 times and pay about the same pressure drop penalty. They also reported that the flatter velocity profile and higher turbulence intensity are responsible for producing higher heat transfer. The use of such roughness on the absorber plate of solar air heater makes the fluid flow and the heat transfer characteristics distinctly different from those found in the case of two roughened walls and four heated walls duct. Prasad and Saini (1988) and Saini and Saini (1997) applied the artificial roughness in the form of circular wires and expanded metal respectively, in the form of artificial roughness on the inner surface of absorber plate of solar air heaters. They reported a considerable enhancement in heat transfer coefficient and friction factor and hence the enhancement of the efficiency of solar air heater.

The objective of the present investigation is to generate friction and heat transfer data pertinent to the heating of air in a rectangular duct with rib-grooved transverse repeated rib roughness on one broad heated wall for Reynolds numbers varying between 3000 and 21,000. The statistical correlations for Nusselt number and friction factor in terms of roughness parameters have been developed and the effect of system and operating parameters has been discussed.

2. Roughness parameters

The roughness parameters are determined by rib height (e), rib pitch (p) and groove position between the ribs (g). These parameters have been expressed in the form of the following dimensionless roughness parameters:

(i) Relative roughness pitch, (p/e).
(ii) Relative roughness height, (e/D).
(iii) Groove position to pitch ratio, (g/p).

The range of these dimensionless roughness parameters and Reynolds numbers employed in this investigation are given below:

(a)	Reynolds number, (Re)	3000–21,000
(b)	Relative roughness height, (e/D)	0.0181–0.0363
(c)	Relative roughness pitch, (p/e)	4.5–10.0
(d)	Groove position to pitch ratio, (g/p)	0.3–0.7

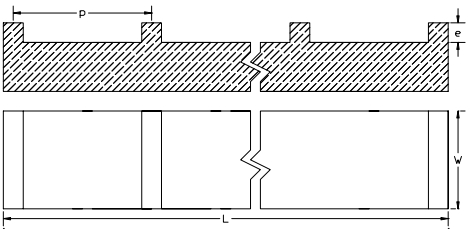

Fig. 1. Rib roughness geometry.

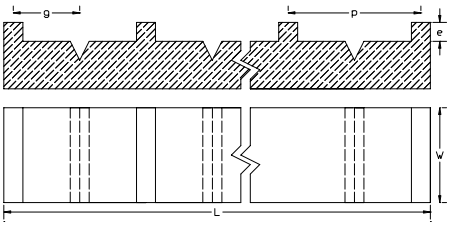

Fig. 2. Rib-groove geometry.

The geometry of ribbed surface and rib-grooved surface is shown in Figs. 1 and 2, respectively.

3. Experimental program

3.1. Experimental setup

An experimental setup has been designed and fabricated to study the effect of rib-grooved geometry on the heat transfer and fluid flow characteristics of air flow in the rectangular duct. A schematic diagram of the experimental setup including test section is shown in Fig. 3. The flow system consists of an entry section, test section, exit section, mixing section, transition section, a flow measuring orifice plate and a centrifugal blower with a control valve. The wooden rectangular duct has internal dimensions of 2420 mm × 156 mm × 22 mm which consists of entrance section, test section and exit section of length 650 mm, 1200 mm and 570 mm, respectively, in accordance with the recommendations of ASHRAE Standard (1977). The exit section of 570 mm length has a mixing chamber formed by introducing three equally spaced baffles in the 100 mm length for the purpose of mixing the delivered air. The outlet temperature of delivered air is measured at 200 mm after the mixing chamber. An electrical heater of size 1200 mm × 156 mm was fabricated by combining series and parallel loops of heating wire on 5 mm asbestos sheet. A 50 mm glass wool was applied as insulation on the backside of heater in

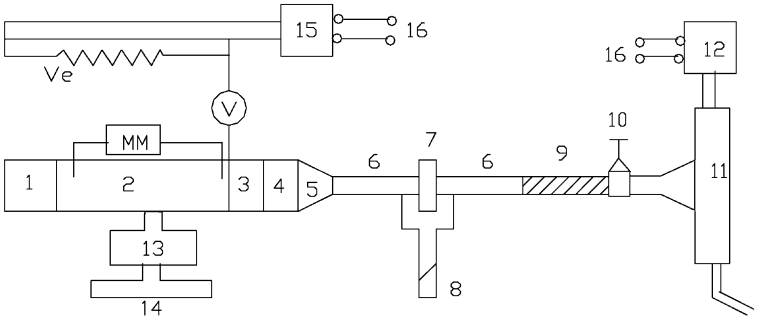

(a) Experimental setup

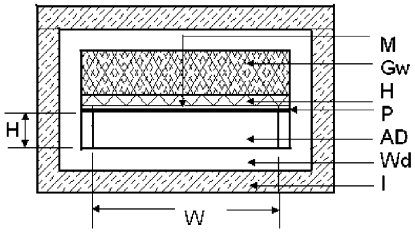

(b) Enlarged view of test cross section

1. Inlet section (560 mm x 156 mm)	11. Blower
2. Test section (1200 mm x 156 mm)	12. Electric motor Selector-switch
3. Mixing section (300 mm x 156 mm)	13. Selector-switch
4. Outlet section (540 mm x 156 mm)	14. Temperature Recorder
5. Transition section	15. Power source
6. G. I. pipe, 78 mm diameter	16. Voltage stabilizer
7. Orificemeter	MM Micro-manometer
8. Manometer	V Volt meter
9. Flexible pipe	A Ammeter
10. Control valve	Ai Air inlet
	Ve Variac

Fig. 3. Schematic diagram of experimental setup.

3 mm plywood box. The heat flux can be varied from 0 to 1200 W/m^2 by a variac transformer. The top side of the entry and the exit sections of the duct is covered with smooth face of 12 mm thick plywood. The heated plate is 3 mm thick aluminum plate with integral rib-grooves alternately formed on the under side which forms the top broad wall of the duct, while other sides are smooth with 25 mm wood with insulation of 50 mm thickness insulation sheet. The mass flow rate of air is measured by means of a calibrated orifice plate connected with inclined U-tube manometer using methyl alcohol as manometer fluid and flow is controlled by the control valves provided in the pipe line. The calibrated copper constantan 28 SWG thermocouples were used to measure the temperature of air and the heated plate at different locations. A digital temperature indicator is used to display the output of the thermocouples. It is calibrated to measure the temperature within $\pm$0.01 °C. The pressure drop across the test section was measured by a micro-manometer having a least count of 0.01 mm. The air is sucked through the rectangular duct by means of a blower driven by a 3-phase, 440 V, 3.73 kW, 2880 rpm AC motor.

3.2. Experimental procedure

Before starting the experiment, all the thermocouples were checked carefully so that they indicate the room temperature and all the pressure tapings were checked for leakage if any. The test runs were conducted under steady state conditions to collect relevant heat transfer and flow friction data. The

steady state condition was assumed to have been reached when the temperature at any location does not change for about 10 min. When a change in the operating conditions is made, it takes about 30 min to reach the steady state. Seven values of flow rates were used for each set at a fixed heat flux of the test. After each change of flow rate, the system is allowed to attain a steady state before the data were recorded. The following parameters were measured:

(i) Temperature of the heated plate.
(ii) Temperature of air at inlet and outlet of the test section.
(iii) Pressure drop across the test section.
(iv) Pressure difference across the orifice meter.

4. Data reduction

Steady state values of the plate and air temperatures in the duct at various locations were used to determine the values of useful parameters, namely mass flow rate "m", heat supplied to the air "Q_u" and heat transfer coefficient "h" calculated as

$$m = C_d A_o \left[\frac{2\rho(\Delta P)_o}{1-\beta^4}\right]^{0.5}, \quad (1)$$

where $(\Delta P)_o = 9.81\rho_m(\Delta h)_o(\sin\theta)$.

$$Q_u = mC_p(T_o - T_i), \quad (2)$$

$$h = \frac{Q_u}{A_p(T_p - T_f)}, \quad (3)$$

where the temperature T_p and T_f are average temperature values of absorber plate and fluid respectively. The average value of plate temperature (T_p) was determined from the detailed temperature profile of the absorber plate indicated by 13 thermocouples at various locations shown in Fig. 4. The

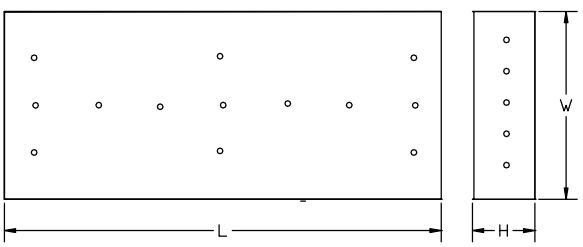

(Distance between two thermocouples along the length, L is 180 mm)

Fig. 4. Location of thermocouples on absorber plate and outlet of duct section.

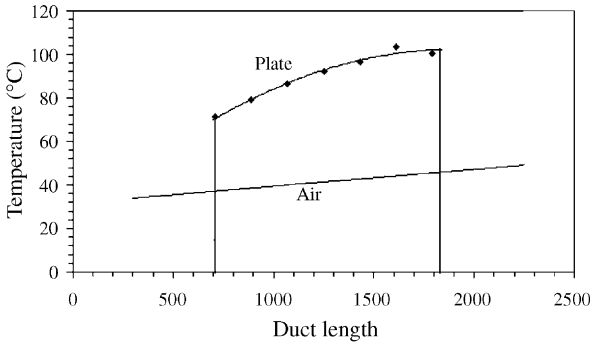

Fig. 5. Variation of plate and air temperature with duct length.

typical variation of the plate and air temperatures along the length of the duct is shown in Fig. 5. The convective heat transfer coefficient was then used to obtain Nusselt number, Nu, as

$$Nu = \frac{h \cdot D}{k}. \quad (4)$$

The friction factor was determined from the measured values of pressure drop, $(\Delta P)_d$, across the test section length, between the two points located 1 m apart; one at 580 mm and other at 1580 mm from the inlet of the duct, as

$$f = \frac{2 \cdot (\Delta P)_d \cdot D}{4 \cdot \rho \cdot L_f \cdot V^2}, \quad (5)$$

where $(\Delta P)_d = 9.81\rho_m(\Delta h)_d$.

It may be noted that prior to actual data collection, the test setup was checked by conducting experiments for a smooth duct. The Nusselt number and friction factor determined from these experimental data were compared with the values obtained from the correlations i.e. Dittus Boelter equation for the Nusselt number (Kays and Perkin, 1990) and modified Blasius equation for the friction factor (Bhatti and Shah, 1987) given below: Dittus Boelter equation:

$$Nu_s = 0.024Re^{0.8}Pr^{0.4}. \quad (6)$$

Modified Blasius equation:

$$f_s = 0.085Re^{-0.25}. \quad (7)$$

The average absolute percentage deviation of the present experimental Nusselt number data is 3.33% from the values predicted by Eq. (6), and the average absolute percentage deviation for friction factor data is 4.40% from the values predicted by Eq. (7) as shown in Figs. 6 and 7. This comparison ensures the accuracy of the experimental data collected with the present setup. From the analysis

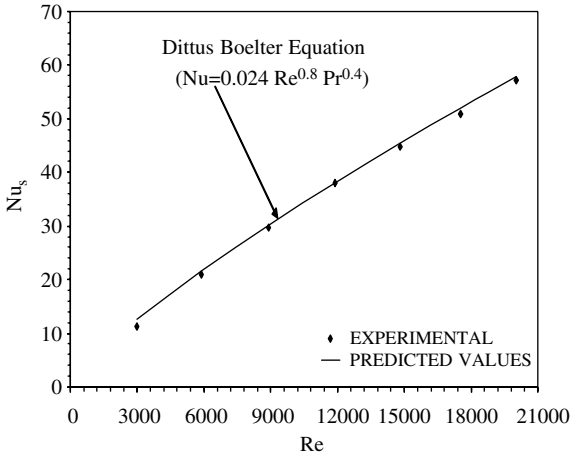

Fig. 6. Nusselt number vs Reynolds number for smooth duct.

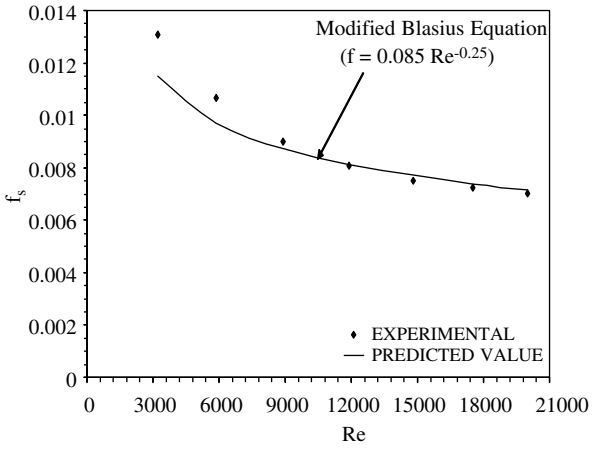

Fig. 7. Friction factor vs Reynolds number for smooth duct.

of the uncertainties in the measurement by various instruments (Klein and McClintock, 1953), the maximum uncertainties in the calculated values of various parameters are Reynolds number = ±2.96%; Nusselt number = ±3.1%; Friction factor = ±6.33%.

5. Results and discussion

Using the data obtained from experiments, the heat transfer, friction factor and the thermal performance characteristics of duct are discussed as follows.

5.1. Heat transfer

Fig. 8 shows the variation of Nusselt number for rib-grooved, ribbed (or ribs only) and smooth duct

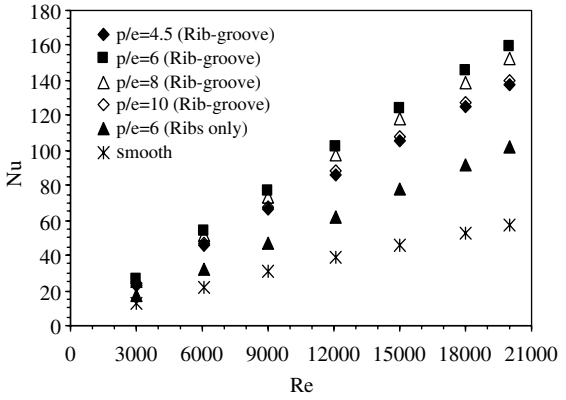

Fig. 8. Nusselt number vs Reynolds number for $e/D = 0.0363$ and $g/p = 0.4$.

with Reynolds number and relative roughness pitch for given values of groove position and relative roughness height. The values of Nusselt number are found to increase with increasing Reynolds number in all cases as expected. The rib-grooved ducts can be seen to yield higher Nusselt number as compared to that of the ribbed duct as is evident from the comparison of two such plots for relative roughness pitch ratio of 6.0. The vortices induced in and around the grooves are thought to be responsible for the increase in the intensity of turbulence which leads to higher heat transfer rate in the case of rib-groove combination. Similar results were obtained by Zhang et al. (1994) who concluded that the flatter velocity profile and higher turbulence intensity in rib-grooved duct are responsible for producing higher heat transfer.

The data of Fig. 8 has been replotted in Fig. 9 to bring out the effect of relative roughness pitch

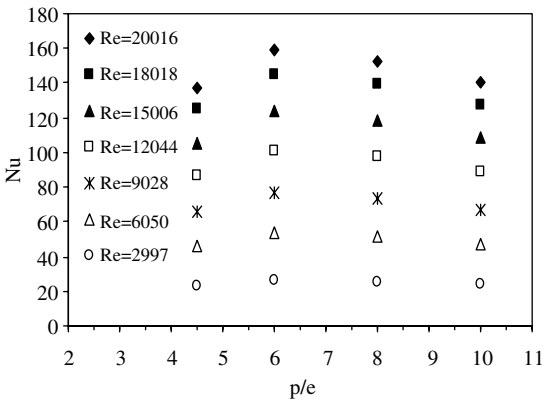

Fig. 9. Nusselt number vs relative roughness pitch for $g/p = 0.4$ and $e/D = 0.0363$.

wherein it can be seen that the Nusselt number increases with increase of relative roughness pitch, attaining maximum value at relative roughness pitch of 6.0 and then decreases with further increase in relative roughness pitch. It is observed from the plot that the variation of Nusselt number with relative roughness pitch is insignificant at lower values of Reynolds number but at higher Reynolds number, the variation is substantial.

The rib-grooved duct with relative roughness pitch of 6.0 provides the highest heat transfer coefficient at all Reynolds numbers. This appears to be due to an optimum combination of pitch, height and groove location; which results in maximum heat transfer.

Fig. 10 shows the effect of the groove position on Nusselt number for rib-grooved duct. It can be seen that the Nusselt number first increases as the groove position to pitch ratio is increased, attaining maximum value at groove position of 0.4 and then decreases with further increase in the value of groove position, the effect being more pronounced at higher values of Reynolds number. Although the plots have been shown for a fixed relative roughness pitch of 6.0, the trend is general and the same trend is seen at all relative roughness pitch values. Fig. 11 shows the plots of Nusselt number as a function of relative roughness height, (e/D) for rib-grooved duct for given values of other roughness geometrical parameters. Plots show a monotonic rise in the value of Nusselt number with an increase in the relative roughness height.

The rib-grooved duct with relative roughness pitch (p/e) of 6.0 and position of groove to pitch ratio (g/p) of 0.4 provides the maximum value of the Nusselt number in the order of 2.75 times of the smooth duct and 1.57 times of ribbed duct whereas for ribbed duct with similar rib height and rib spacing provides the Nusselt number values of the order of 1.7 times of the smooth duct for the range of experimentation.

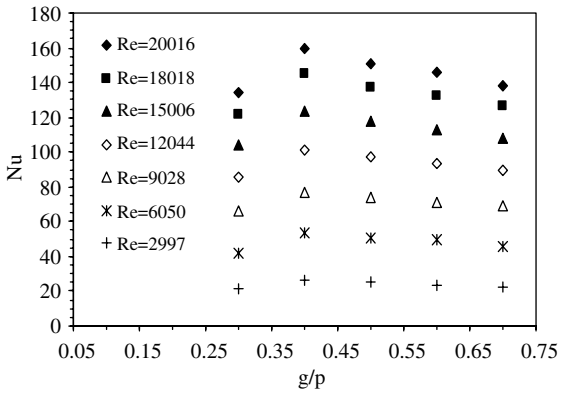

Fig. 10. Nusselt number vs groove position for $p/e = 6$ and $e/D = 0.0363$.

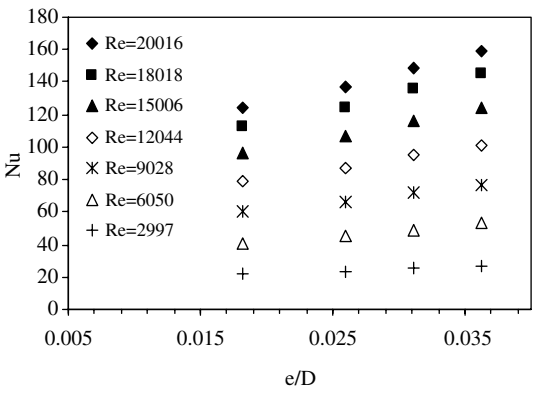

Fig. 11. Nusselt number vs relative roughness height for $p/e = 6$ and $g/p = 0.4$.

5.2. Friction factor

Fig. 12 shows the effect of Reynolds number and relative roughness pitch on friction factor in the range of Reynolds number investigated for fixed value of other parameters. It is seen that the value of friction factor decreases with increasing Reynolds number in all cases as expected due to the suppression of viscous sub-layer with increase in Reynolds number. The rib-grooved ducts can be seen to yield higher friction factor as compared to that of the ribs

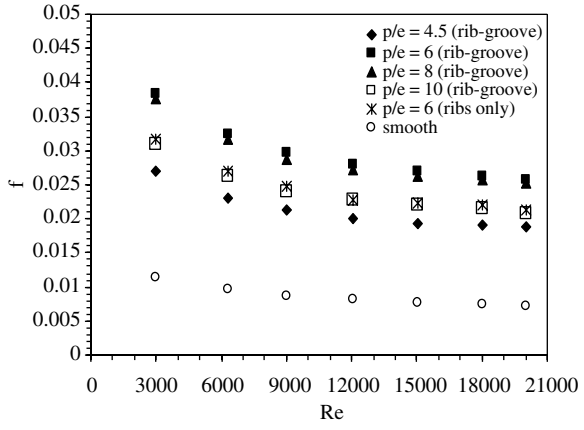

Fig. 12. Friction factor vs Reynolds number for g/p of 0.4 and $e/D = 0.0363$.

only duct as is evident from the comparison of two such plots for relative roughness pitch ratio of 6.0. It is observed that for a relative roughness pitch of 6.0 has maximum friction factor and that of 4.5 has minimum value. The data of Fig. 12 has been replotted in Fig. 13 wherein it can be seen that the friction factor increases with increase in relative roughness pitch, attaining maximum value at relative roughness pitch of 6.0 and a further increase of relative roughness pitch results in the decrease of friction factor; this effect being more pronounced at higher Reynolds number.

Fig. 14 shows the effect of groove position on friction factor in the range of Reynolds number investigated and for fixed values of other parameters. It shows that the value of friction factor for rib-grooved duct with groove position to pitch ratio (g/p) of 0.4 yields the maximum value and decreases on either side. Fig. 15 shows the effect of relative roughness height on the friction factor for fixed values of other roughness and flow parameters. It reveals that there is a monotonic rise in the value of friction factor with the increase in the relative roughness height for a given value of Reynolds number.

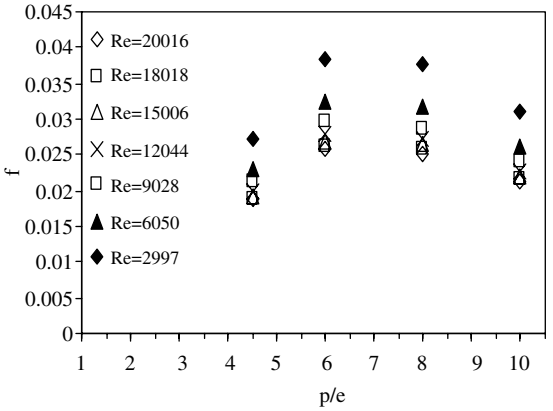

Fig. 13. Friction factor vs relative roughness pitch for $g/p = 0.4$ and $e/D = 0.0363$.

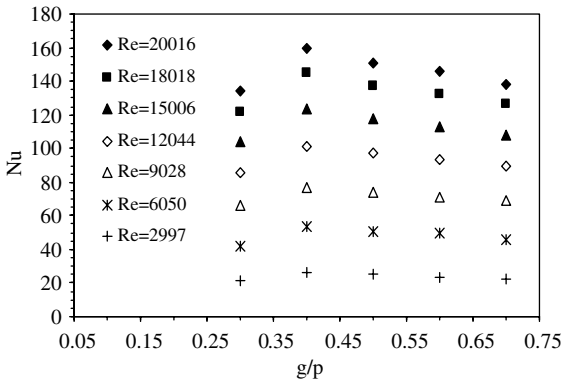

Fig. 14. Friction factor vs groove position for $p/e = 6$ and $e/D = 0.0363$.

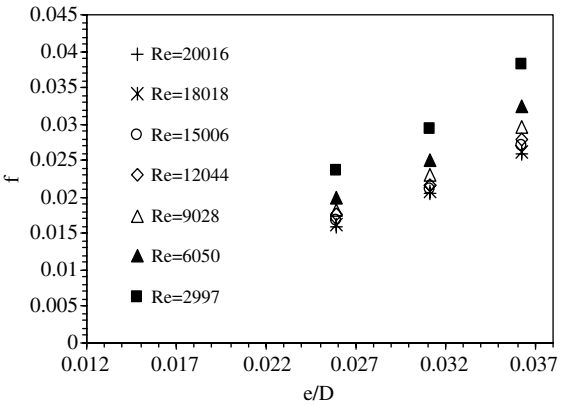

Fig. 15. Friction factor vs relative roughness height for $p/e = 6$ and $g/p = 0.4$.

The investigation shows that the rib-grooved duct with relative roughness pitch (p/e) of 6.0, groove position to pitch ratio (g/p) of 0.4 and relative roughness height (e/D) of 0.0363 yields the maximum value of the friction factor in the order of 3.61 times that of the smooth duct and 1.17 times that of ribbed duct whereas a ribbed duct with similar rib height and rib spacing results in the friction factor value of the order of 3.00 times that of the smooth duct.

5.3. Thermo-hydraulic performance of roughened duct

Thermal performance of a solar air heater duct, in general, gets improved as the flow rate is increased. However, the incremental rise in energy collection declines appreciably at higher Reynolds number whereas the friction losses increase monotonously with an increase in mass flow rate (Thakur, 2001). It is therefore possible that at higher mass flow rates, net energy gain may be less due to proportionately greater energy expenditure required to propel air through the collector. Hence it is necessary that while evaluating the performance of a solar collector with respect to the enhancement of thermal gain, the energy spent in propelling air should also be taken into account. One of the criteria for evaluating the performance of an enhanced

surface is to compare the heat transfer of rib-grooved duct to that of a smooth wall duct under constant pumping power constraints as suggested by Webb and Eckert (1972) and Han et al. (1985). In view of their discussion, an efficiency index $\frac{Nu/Nu_s}{(f/f_s)^{1/3}}$ can decide whether or not a given ribbed surface is potentially gainful. Fig. 16 shows the comparison of thermo-hydraulic performance of rib-grooved ducts and ribbed duct. The result shows that the performance of rib-grooved duct is superior as compared to that of the ribbed duct. For all values of Reynolds number, the thermo-hydraulic performance is maximum for a relative roughness pitch of 6.0. Similarly Fig. 17 shows that for a relative roughness pitch of 6 (for rib-groove), the best thermo-hydraulic performance is obtained for a groove location to pitch ratio of 0.4. It is found that rib-grooved arrangement provides superior thermo-hydraulic performance and hence can be employed for heat transfer augmentation.

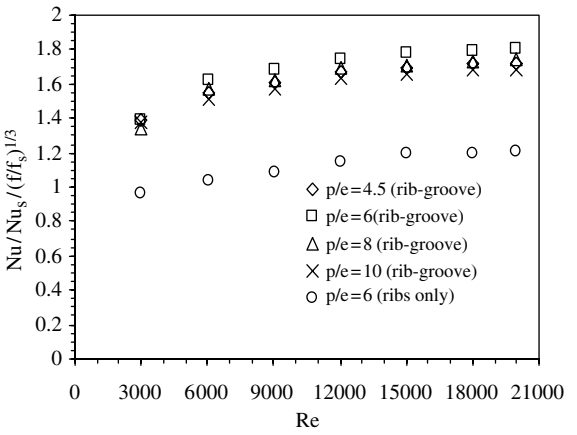

Fig. 16. Variation of $Nu/Nu_s/(f/f_s)^{1/3}$ with Reynolds number for $g/p = 0.4$ and $e/D = 0.0363$.

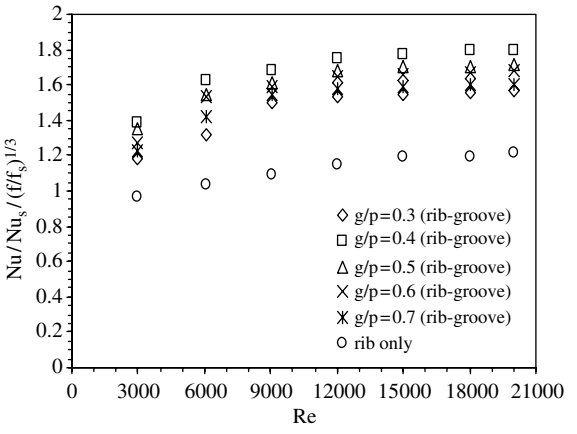

Fig. 17. Variation of $Nu/Nu_s/(f/f_s)^{1/3}$ with Reynolds number for $p/e = 6$ and $e/D = 0.0363$.

6. Correlation for Nusselt number

A statistical correlation is developed on the basis of regression analysis of the experimental data obtained in this work. Fig. 18 shows a plot of Nusselt number as a function of Reynolds number for the entire data of rib-grooved roughness. A regression analysis to fit a straight line on log–log plot through the data points yields the following power law relation between Nusselt number and Reynolds number:

$$Nu = A_0(Re)^{0.936}. \tag{8}$$

The coefficient A_0 will in fact be a function of other influencing parameters. Now taking the parameter of relative roughness height of rib (i.e. e/D) into consideration, the value of $(Nu/(Re)^{0.936} = A_0)$ corresponding to all values of e/D are plotted against (e/D), as shown in Fig. 19. The regression analysis to fit a straight line on log–log scale through points yields:

$$\frac{Nu}{(Re)^{0.936}} = B_0\left(\frac{e}{D}\right)^{0.349}. \tag{9}$$

The coefficient B_0 in Eq. (9) is a function of other influencing parameters. Now considering the parameter relative roughness pitch (p/e), the value of $\frac{Nu}{(Re)^{0.936}(e/D)^{0.349}} = (B_0)$ has been plotted against

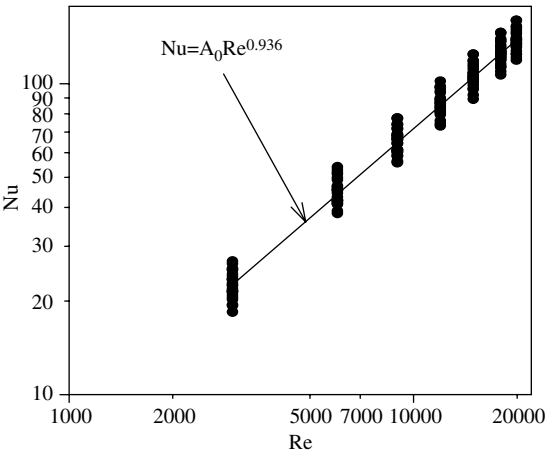

Fig. 18. Plot of Nusselt number vs Reynolds number.

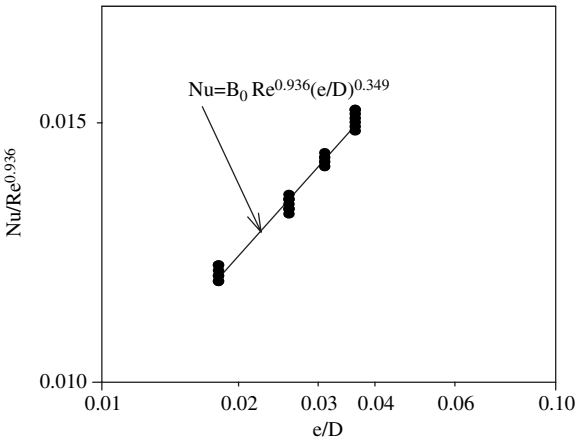

Fig. 19. Plot of $Nu/[Re^{0.936}]$ vs e/D.

relative roughness pitch, (p/e) in Fig. 20. From the regression to fit a second-order quadratic on log–log scale through these points, one obtains

$$\ln\left[\frac{Nu}{(Re)^{0.936}(e/D)^{0.349}}\right] = \ln C_0 + C_1(\ln(p/e)) + C_2(\ln(p/e))^2. \quad (10)$$

Eq. (10) can be rearranged as

$$\frac{Nu}{(Re)^{0.936}(e/D)^{0.349}} = C_0(p/e)^{C_1}(\exp(C_2\cdot(\ln(p/e))^2)). \quad (11)$$

Using the values of C_1 and C_2 obtain from regression

$$\frac{Nu}{(Re)^{0.936}(e/D)^{0.349}} = C_0(p/e)^{3.318}\exp(-0.868(\ln(p/e))^2), \quad (12)$$

where C_0 is a function of parameter representing groove position to pitch ratio. Finally a plot of $\ln\left(\frac{Nu}{(Re)^{0.936}(e/D)^{0.349}(p/e)^{3.318}\exp(-0.868(\ln(p/e))^2)}\right) = C_0$ as a function of g/p, shown in Fig. 21 has been used to fit a third order quadratic on log–log scale through these points, given as

$$\ln\left(\frac{Nu}{(Re)^{0.936}\left(\frac{e}{D}\right)^{0.349}\left(\frac{p}{e}\right)^{3.318}\exp\left(-0.868\left\{\ln\left(\frac{p}{e}\right)\right\}^2\right)}\right) = \ln D_0 + D_1\left(\ln\left\{\frac{g}{p}\right\}\right) + D_2\left(\ln\left\{\frac{g}{p}\right\}\right)^2 + D_3\left(\ln\left\{\frac{g}{p}\right\}\right)^3, \quad (13)$$

where $D_0 = 0.002062$, $D_1 = 1.108$, $D_2 = 2.486$, $D_3 = 1.406$ as obtained from regression.

Eq. (13) can be re-arranged as

$$\frac{Nu}{(Re)^{0.936}\left(\frac{e}{D}\right)^{0.349}\left(\frac{p}{e}\right)^{3.318}\exp\left(-0.868\left\{\ln\left(\frac{p}{e}\right)\right\}^2\right)} = 0.002062\left(\frac{g}{p}\right)^{1.108}\exp\left[2.486\left\{\ln\left(\frac{g}{p}\right)\right\}^2 + 1.406\left\{\ln\left(\frac{g}{p}\right)\right\}^3\right]. \quad (14)$$

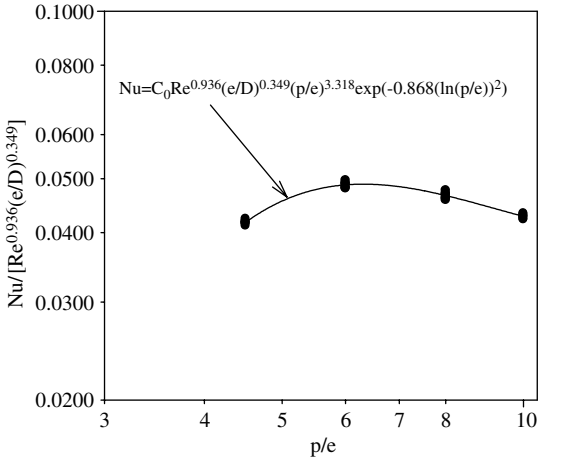

Fig. 20. Plot of $Nu/[Re^{0.936}(e/D)^{0.349}]$ vs p/e.

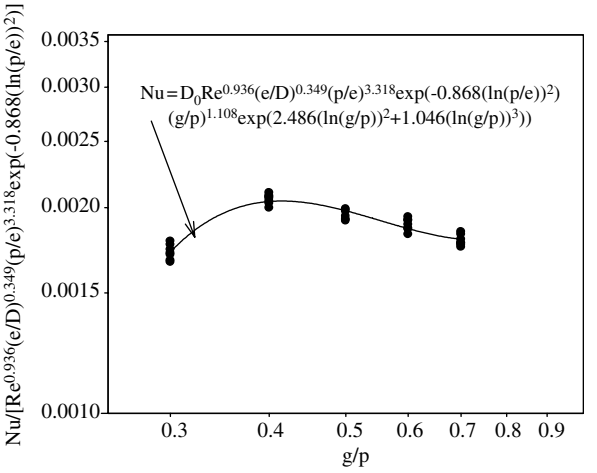

Fig. 21. Plot of $Nu/[Re^{0.936}(e/D)^{0.349}(p/e)^{3.318}\exp(-0.868(\ln(p/e))^2]$ vs g/p.

Finally, Eq. (14) yields the following correlation for Nusselt number.

$$Nu = 0.002062Re^{0.936}\left(\frac{e}{D}\right)^{0.349}\left(\frac{p}{e}\right)^{3.318} \times \exp\left[-0.868\left\{\ln\left(\frac{p}{e}\right)\right\}^2\right]\left(\frac{g}{p}\right)^{1.108} \times \exp\left[2.486\left\{\ln\left(\frac{g}{p}\right)\right\}^2 + 1.406\left\{\ln\left(\frac{g}{p}\right)\right\}^3\right]. \quad (15)$$

7. Correlation for friction factor

A similar method has been employed to develop a correlation for the friction factor.

The final correlation for friction factor that has been developed based on data plotted in Figs. 22–25 can be written in the following form:

$$f = 0.001227(Re)^{-0.199}\left(\frac{e}{D}\right)^{0.585}\left(\frac{p}{e}\right)^{7.19}\left(\frac{g}{p}\right)^{0.645} \times \exp\left(-1.854\left\{\ln\left(\frac{p}{e}\right)\right\}^2\right) \times \exp\left(1.513\left\{\ln\left(\frac{g}{p}\right)\right\}^2 + 0.8662\left\{\ln\left(\frac{g}{p}\right)\right\}^3\right). \quad (16)$$

Figs. 26 and 27 show the comparison of the experimental values of Nusselt number and friction factor with those predicted by the respective correlations as given in Eqs. (15) and (16). Fig. 26 shows 98% of the data points lying within ±10% and the average absolute percentage deviation has been found to be 2.73% while Fig. 27 shows 96% of data points lie within ±8%. The average absolute percentage deviation for this case is 3.16%.

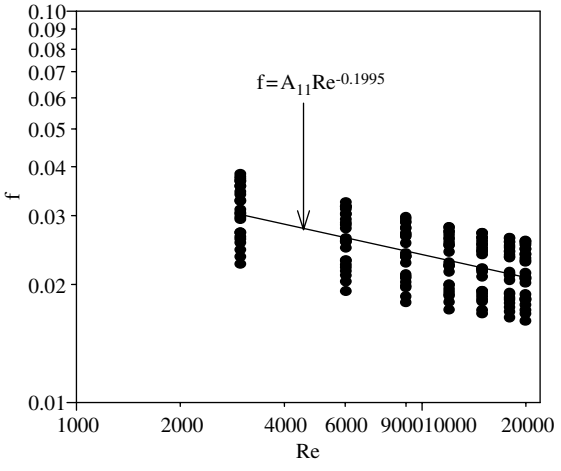

Fig. 22. Plot of friction factor vs Reynolds number.

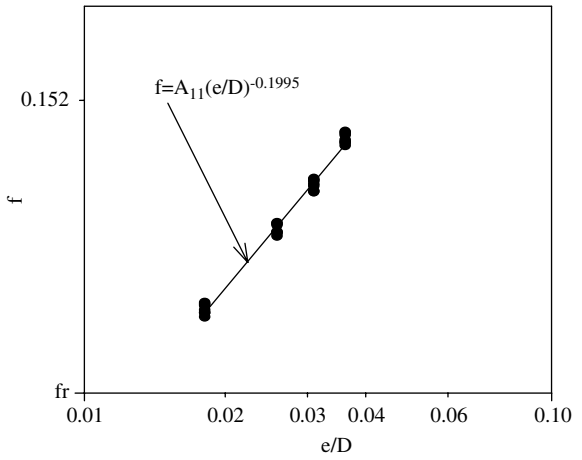

Fig. 23. Plot of $f/[Re^{-0.1995}]$ vs e/D.

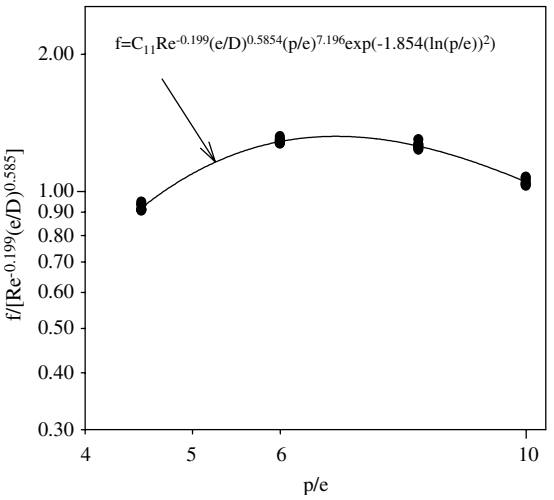

Fig. 24. Plot of $f/[Re^{-0.1995}(e/D)^{0.5854}]$ vs p/e.

8. Conclusions

The effect of rib-grooved artificial roughness on the heat transfer coefficient, friction factor and thermo-hydraulic performance of the solar air heater duct having one principal wall roughened with rib-groove has been investigated. The effect of relative roughness pitch, relative roughness height and relative groove position on the heat transfer

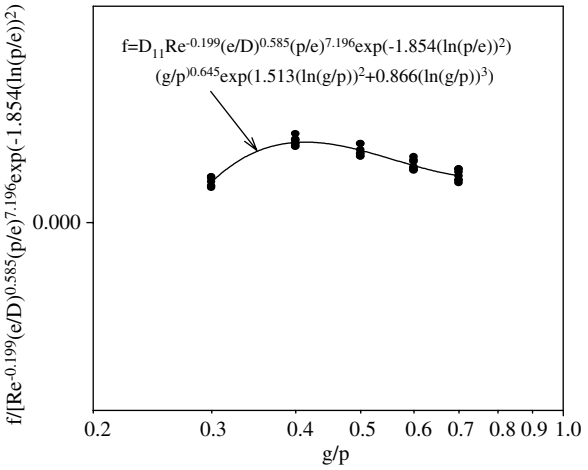

Fig. 25. Plot of $f/[Re^{-0.1995}(e/D)^{0.5854}(p/e)^{7.196}\exp(-1.854(\ln(p/e))^2]$ vs g/p.

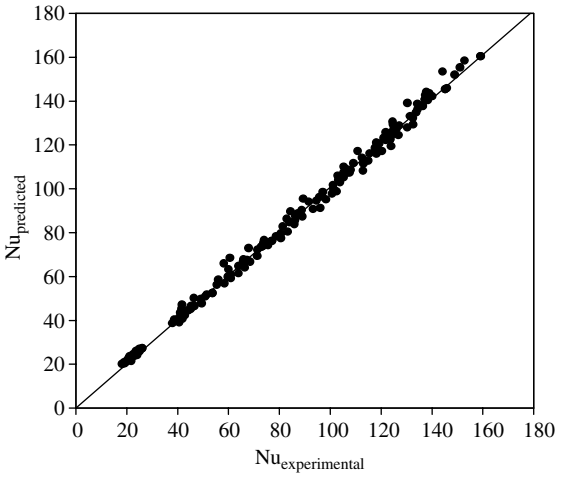

Fig. 26. Comparison of experimental values of Nusselt number with those predicted by the correlation (Eq. (15)).

coefficient and friction factor has been studied. The major conclusions are

(i) As compared to the smooth duct, the presence of rib grooved artificial roughness yields Nusselt number up to 2.7 times while the friction factor rises up to 3.6 times in the range of parameters investigated.
(ii) The maximum heat transfer occurs for a relative roughness pitch of about 6.0, and it decreases either side of relative roughness pitch and similar trend is observed for friction factor.

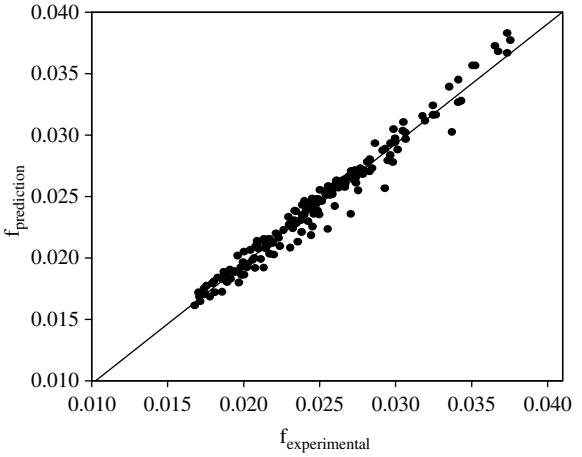

Fig. 27. Comparison of experimental values of friction factor with those predicted by the correlation (Eq. (16)).

(iii) The optimum condition for heat transfer occurs at a groove position to pitch ratio of 0.4, while on the either side of this ratio, both Nusselt number and friction factor decreases.
(iv) Statistical correlations for Nusselt number and friction factor have been developed as a function of rib-groove position, rib height (or depth), pitch and Reynolds number. These correlations have been found to predict the values of Nusselt number and friction factor with average absolute percentage deviation of 2.73% and 3.16% respectively.
(v) It is found that the rib-grooved arrangement provides the best thermo-hydraulic performance and hence can be employed for heat transfer augmentation.

References

ASHRAE Standard, 93-77, 1977. Methods of testing to determine the thermal performance of solar collectors.

Bhatti, M.S., Shah, R.K., 1987. Turbulent and transition convective heat transfer in ducts. In: Kakac, S., Shah, R.K., Aung, W. (Eds.), Hand Book of Single Phase Convective Heat Transfer. Wiley, New York, pp. 4.1–4.166.

Dipprey, D.P., Sabersky, R.H., 1963. Heat and momentum transfer in smooth and rough tubes at various Prandtl numbers. Int. J. Heat Mass Transfer. 6, 329–353.

Han, J.C., Park, J.S., 1988. Developing heat transfer in rectangular channels with rib turbulators. Int. J. Heat Mass Transfer 3/1, 183–195.

Han, J.C., Park, J.S., Lei, C.K., 1985. Heat transfer enhancement in channel with turbulence promoters. Trans. ASME J. Eng. Gas Turbines Power 107, 628–635.

Han, J.C., Park, J.S., Lei, C.K., 1989. Augmented heat transfer in rectangular channel of narrow aspect ratios with rib turbulators. Int. J. Heat Mass Transfer 32/9, 1619–1630.

Kays, W.M., Perkin, H., 1990. Forced convection internal flow in ducts. In: Rohsenow, W.M., Hartnett, I.V. (Eds.), Hand Book of Heat Transfer. McGraw-Hill, New York.

Klein, S.J., McClintock, A., 1953. The description of uncertainties in single sample experiments. Mech. Eng. 75, 3–8.

Nikuradse, J., 1950. Law of flow in rough pipes, National Advisory Committee for Aeronautics Technical Memorandum 1292.

Prasad, B.N., Saini, J.S., 1988. Effect of artificial roughness on heat transfer and friction factor in a solar air heater. Sol. Energy 41/6, 555–560.

Saini, J.S., 2004. Use of artificial roughness for enhancing performance of solar air heater. In: Proceedings of XVII National and VI ISHME/ASME Heat Mass Transfer Conference, IGCAR, Kalpakkam (India), pp. 103–112.

Saini, R.P., Saini, J.S., 1997. Heat transfer and friction factor correlations for artificially roughened ducts with expanded metal mesh as roughness element. Int. J. Heat Mass Transfer 40/4, 973–986.

Thakur, N.S., 2001. Thermo-hydraulic performance and optimization of packed bed solar air heater. A Ph.D. Thesis, Dept. of Mechanical and Ind. Eng., University of Roorkee, Roorkee (India).

Webb, R.L., 1987. Enhancement of single phase heat transfer. In: Kakac, S., Shah, R.K., Aung, W. (Eds.), Hand Book of Single Phase Convective Heat Transfer. Wiley, New York, pp. 17.1–17.8.4.

Webb, R.L., Eckert, E.R.G., 1972. Application of rough surface to heat exchanger design. Int. J. Heat Mass Transfer 15, 1647–1658.

Webb, R.L., Eckert, E.R.G., Goldstein, R.J., 1971. Heat transfer and friction in tubes with repeated rib roughness. Int. J. Heat Mass Transfer 14, 601–617.

Zhang, Y.M., Gu, W.Z., Han, J.C., 1994. Heat transfer and friction in rectangular channels with ribbed or ribbed-grooved walls. Trans. ASME J. Heat Transfer 116, 58–65.